



Verification and validation of numerical solutions of two-dimensional reactive flow in rocket engine nozzles



Luciano Kiyoshi Araki*, Carlos Henrique Marchi

Federal University of Paraná—UFPR, Department of Mechanical Engineering (DEMEC), 81531-980 Curitiba, PR, Brazil

ARTICLE INFO

Article history:

Received 10 September 2015
 Revised 15 July 2017
 Accepted 24 July 2017
 Available online 28 July 2017

Keywords:

Finite volume method
 Non-orthogonal grid
 H_2/O_2
 Numerical error estimate
 Verification
 Nozzle

ABSTRACT

Two-dimensional mathematical models for gaseous H_2/O_2 reactive flows are solved for two geometries: a conical and a parabolic one. Five different physical models are studied: two one-species and three multi-species models (frozen, equilibrium and non-equilibrium flows). In the mathematical model, temperature is used as unknown in the energy equation and velocity is obtained for all speed flows. For all analyses, a non-orthogonal finite volume code was implemented, taking into account first (UDS) and second (CDS) order interpolation schemes and co-located grid arrangement. Model predictions of the pressure distribution and Mach number in the nozzle with a conical geometry, calculated using a CDS scheme, were found to agree well with experimental results. For both geometries, numerical results for apparent orders of convergence agreed well with the asymptotic (expected) ones for one-species flows. Some other analyses were provided for mixture of gases flows; in this case, for frozen flow, the apparent order values tend to the asymptotic ones in all cases; for local equilibrium flow, the use of CDS degenerated the apparent order to unity; this fact can be associated to the use of UDS interpolation scheme in the source term of the energy equation. Numerical solutions, including their error estimates, are provided for UDS and CDS schemes. Their analysis shows that global variables of interest (such as thrust and specific impulse) are less affected by the chosen physical model than are local variables of interest (such as the temperature at the symmetry line).

© 2017 Published by Elsevier Inc.

1. Introduction

The effort to increase the reliability of rocket engines should span the entire program spectrum from conceptual design to its production. The reliability effort can basically be divided into three parts: prevention of failures, process assessment and control, and monitoring of performance [1]. One important reason for the failure of the wall material is the high temperature values achieved in it. Thus, this is the major reason for studies involving heat transfer throughout the rocket engine nozzle. In order to study the heat transfer phenomena it is essential to be familiar with aspects related to the reactive gas flow through the entire nozzle.

Many papers about heat transfer and reactive gas flow in rocket engine nozzles have been published in the past, including: fluid–structure interactions in regenerative cooling systems [2]; reactive gas flow and regenerative cooling system [3]; two- and three-dimensional turbulent flows and irradiative heat transfer [4]; liquid film cooling effects [5]; and the start-up side load analysis in a regeneratively cooled nozzle [6]. Although some of these works are concerned with numerical

* Corresponding author.

E-mail addresses: lucaraki@ufpr.br, lucianoaraki@gmail.com (L.K. Araki), marchi@ufpr.br (C.H. Marchi).

validation, including comparisons between numerical results and experimental data, none of them provides results with a numerical verification approach.

Unfortunately, numerical error analysis for supersonic flows is not a common practice: none of the studies cited above employed numerical tools to provide numerical error estimates, nor even mentioned the orders of numerical error. This may be related to the fact that the theoretical foundation of a posteriori and a priori error analysis is far from satisfactory for nonlinear hyperbolic problems [7], such as supersonic flows. Moreover, despite its importance in practical applications, only in recent years have the difficulties in estimating numerical errors and its control received sufficient attention [7].

According to Oberkampf and Trucano [8], verification and validation are the primary means of assessing the accuracy and reliability of computational simulations. While validation is associated with the accuracy of a mathematical model in relation to a real physical phenomenon, verification consists of the quantification of the numerical error [9–10].

Therefore, the purposes of the current work are: (1) to validate a numerical code for two-dimensional compressible reactive and non-reactive flows; (2) to provide a posteriori error analyses for reactive compressible flows, by the comparison between the asymptotic and the apparent orders and also by the use of the Grid Convergence Index (GCI) for the numerical error estimates [11]; and (3) to compare the performance of six and eight species models for chemical reaction schemes, related to the rocket engine parameters and the processing (CPU) time requirements.

In order to achieve the cited aims, the numerical model presents the following features: the use of the Finite Volume Method [12], co-located non-orthogonal grids, a methodology appropriate to all speed flows [13], a temperature-based energy conservation equation and different physical models, which include one and multi-species flows; for multi-species flows, different chemical reaction schemes can be chosen. The implemented code also allows the use of the following interpolation schemes: Upstream Differencing Scheme (UDS), Central Differencing Scheme (CDS) with deferred correction [14], or even a hybrid scheme. Although the focus of the numerical results is the achievement of steady flow, time is used, in a totally implicit form, as a relaxation parameter.

By using the methodology proposed by Marchi and Maliska [13], the numerical code provides results for all flow regimes into the rocket engine nozzle (sub-, trans- and supersonic ones), unlike the commonly used method of characteristics [15–16], which can be used only for hyperbolic problems (correspondent to supersonic flows). And unlike the MacCormack method, which is also widely used for nozzle flow studies [15], the implemented code presents a totally implicit methodology, and not an explicit one. The implemented code also allows detection of oblique shocks, which can be seen by the analysis of isolines for Mach number, temperature or pressure.

In next Section (Section 2) is presented the mathematical model; details of the discretization and the algorithm used are given in Section 3. Some basic information about verification is presented in Section 4, while geometry, boundary conditions and associated information are given in Section 5. Numerical results and their discussion are provided in Section 6 and the final remarks are exposed in Section 7.

2. Mathematical model

The basic principles involved in rocket propulsion science are essentially those of mechanics, thermodynamics and chemistry [17]. In rocket engines with regenerative cooling systems, the whole thrust mechanism can be divided into three different (but coupled) problems, for which there are independent mathematical (and numerical) models [18–20]: (1) the flow of the reaction gas products (combustion gases mixture) through the thrust chamber; (2) the heat conduction from hot gases to the coolant; and (3) the coolant flow through the regenerative cooling system.

According to Anderson Jr [15] and John and Keith [21], there are a number of important applications that do not involve flows with large gradients that can readily be assumed to be non-viscous, which includes flows in rocket engine nozzles. Based on this, the focus of this work is, however, only the flow of combustion products, which can be modeled by the mass conservation, two-dimensional momentum and energy equations (together representing the steady axisymmetric Euler equations), and a state relation, as follows:

$$\nabla \cdot (\rho \mathbf{V}) = 0 \quad (1)$$

$$\nabla \cdot (\mathbf{V} \times \rho \mathbf{V}) = -\nabla P \quad (2)$$

$$\nabla \cdot (\rho \mathbf{V} T) = \frac{1}{c_p} [\nabla \cdot (P \mathbf{V}) - P \nabla \cdot \mathbf{V}] + S_{eq/ne} \quad (3)$$

$$P = \rho R T \quad (4)$$

where: ρ , \mathbf{V} , P and T are the dependent variables, which correspond to density, velocity vector (whose components are u and v , in axial and radial directions, in this order), pressure and temperature, respectively; c_p is the frozen specific heat (which must be evaluated for each control volume, for reactive flows); R is the one-species constant or multi-species mixture constant; $\nabla \cdot \mathbf{A}$ is the divergence operator applied on an \mathbf{A} vector; and $S_{eq/ne}$ is the chemical source term. Temperature is taken as the primary dependent variable since, according to Bird et al. [22], the most useful form of the energy equation is one in which temperature appears. Furthermore, Murthy and Mathur [23] affirm that it is desirable to have both the

Table 1
Chemical reaction schemes implemented in Mach2D 6.0 code.

Model	<i>L</i>	<i>N</i>	Species	Observations
0	0	3	H ₂ O, O ₂ , H ₂	Ideal model
1	1	3	H ₂ O, O ₂ , H ₂	–
2	2	4	H ₂ O, O ₂ , H ₂ , OH	–
3	4	6	H ₂ O, O ₂ , H ₂ , OH, O, H	4 reactions with 3rd body—Barros et al. [25] and Smith et al. [26]
4	4	6	H ₂ O, O ₂ , H ₂ , OH, O, H	4 reactions—Svehla [27]
5	8	6	H ₂ O, O ₂ , H ₂ , OH, O, H	8 reactions (4 with 3rd body)—Barros et al. [25]
7	8	6	H ₂ O, O ₂ , H ₂ , OH, O, H	8 reactions (4 with 3rd body)—Smith et al. [26]
9	18	8	H ₂ O, O ₂ , H ₂ , OH, O, H, HO ₂ , H ₂ O ₂	18 reactions (5 with 3rd body)—Kee et al. [28]
10	6	8	H ₂ O, O ₂ , H ₂ , OH, O, H, HO ₂ , H ₂ O ₂	4 reactions from model 3 and 2 from Kee et al. [28]—all the reactions including 3rd body

right and the left-hand sides of the equation expressed in terms of the same dependent variable, either total enthalpy or temperature. They also affirm that formulations using enthalpy as the dependent variable must recover temperature from enthalpy after enthalpy is computed; besides the boundary conditions are most naturally written in terms of temperature, which means this parameter is preferable for use in the mathematical model. The chemical source term, $S_{eq/ne}$ in Eq. (3), is null for all cases, except for the local equilibrium flow model, for which it is evaluated by:

$$S_{eq/ne} = -\frac{1}{c_p} \left[\sum_{i=1}^N h_i \nabla \cdot (\rho \mathbf{V} Y_i) \right] \quad (5a)$$

and for the non-equilibrium flow model, for which it is estimated by:

$$S_{eq/ne} = -\frac{1}{c_p} \sum_{i=1}^N h_i \dot{w}_i \quad (5b)$$

In Eq. (5), N is the total number of chemical species; Y_i , h_i and \dot{w}_i are, in this order, the mass fraction, the enthalpy and the generation rate for a given chemical species i . Enthalpy is evaluated using temperature and interpolation polynomials, given by McBride et al. [24]. Considering the non-equilibrium flow, another equation must be taken into account: the species continuity equation,

$$\nabla \cdot (\rho \mathbf{V} Y_i) = \dot{w}_i \quad (6)$$

This equation is not used for frozen and local equilibrium models, since for them a simple balance of species, based on the mass fraction of each species, is enough to guarantee mass conservation. On the other hand, for non-equilibrium flows, Eq. (6) is needed because equilibrium conditions are not achieved and, because of this, mass generation rates for each species must be evaluated; the species mass conservation depends on these rates. For all three reactive flows (frozen, local equilibrium and non-equilibrium), however, the sum of the considered chemical species in each control volume was verified and had to be equal to the unity. Actually, this condition is imposed at each iteration of the chemical evaluation process, in order to guarantee the mass conservation for all chemical species.

The chemical reaction schemes used in this work for frozen and local equilibrium flows are summarized in Table 1; in this Table, L refers to the number of dissociation reactions related to each chemical model. For the non-equilibrium model, only six and eight reaction scheme models were considered. These are the same chemical reaction schemes previously used [29,30]. These two references present, in this order, the thermochemical properties for oxygen/hydrogen reaction schemes and the complete one-dimensional problem.

3. Numerical model

The presented mathematical model for reaction gas products is discretized using the Finite Volume Method [12] for non-orthogonal grids (transformed ξ - η coordinate system) [13]; in this case, the original system of differential equations given by the mass, momentum, energy and species equations can be rewritten in a general form as:

$$\frac{1}{J} \frac{1}{r} \frac{\partial}{\partial \xi} (r \rho U \Phi) + \frac{1}{J} \frac{1}{r} \frac{\partial}{\partial \eta} (r \rho V \Phi) = -\hat{P}^\Phi + \hat{S}^\Phi \quad (7)$$

in which: Φ is the variable of interest and is listed in Table 2; J is the Jacobian matrix; U and V are the contravariant velocity components; \hat{P}^Φ and \hat{S}^Φ are terms that are listed in Table 2.

For the numerical model, the nozzle geometry is divided into N_z control volumes in the axial direction z and into N_r volumes in the radial direction r . A co-located grid arrangement, as well as a formulation appropriate to all speed flows [13], is used, associated with a first-order (UDS), a second-order (CDS), or a hybrid order (between UDS and CDS) interpolation scheme; for the second-order, so as to allow a better convergence, deferred correction [14] was employed. The systems of algebraic equations obtained by the discretization process are solved by the MSI (Modified Strong Implicit) method [31].

Table 2
Symbols for the general transformed equation (Eq. 7).

Consevation equation	Φ	\hat{P}^Φ	\hat{S}^Φ
Mass	1	0	0
Axial momentum	U	$\frac{\partial P}{\partial \xi} r_\eta - \frac{\partial P}{\partial \eta} r_\xi$	0
Radial momentum	V	$\frac{\partial P}{\partial \eta} z_\xi - \frac{\partial P}{\partial \xi} z_\eta$	0
Energy	T	0	$\frac{1}{j c_p} [\nabla \cdot (P\mathbf{V}) - P\nabla \cdot \mathbf{V}] + S_{eq/me}$
Species	Y_i	0	$\frac{w_i}{J}$

Pressure and velocity are coupled by the SIMPLEC algorithm [32], in order to convert the mass equation to a pressure (or better, in a pressure-correction) one. So, the mass conservation equation, Eq. (1), is used for determination of a pressure-correction (P'). The use of a variant of the SIMPLE algorithm (in this case, the SIMPLEC) is based on the results presented by Demirdzic et al. [33]. In such work, extensive tests for studies involving compressible flows showed stable and good convergence properties. The axial and radial velocity components, (u) and (v), are obtained from the momentum equation, Eq. (2). The energy equation, Eq. (3), is taken for temperature (T) determination. Density (ρ) is determined from the state equation, Eq. (4), while Eq. (6) is also needed for the non-equilibrium flow. It must be noted that the axial velocity (u) is evaluated not only for supersonic flows as commonly found in literature by using the method of characteristics [15–16], but also for subsonic flows of very small velocities.

An algorithm for the reactive two-dimensional reaction gas products flow is presented in the following.

3.1. Algorithm

1. Data reading, grid generation and evaluation of metrics.
2. Estimation of all variables in an instant $t+\Delta t$ (time, however, is only used as a relaxation parameter).
3. Estimation of the inlet pressure and temperature; definition of the frozen constant-pressure specific heat; this value is used as start-up for frozen, local equilibrium and non-equilibrium flows, being re-evaluated on each iteration of the determination process of chemical mass fractions.
4. Discretization of the axial momentum equation providing the coefficients and source-terms of an algebraic system. Evaluation of the axial velocity component u by using the MSI solver.
5. Discretization of the radial momentum equation providing the coefficients and source-terms of an algebraic system. Evaluation of the axial velocity component v by using the MSI solver.
6. Discretization of the energy equation providing the coefficients and source-terms of an algebraic system. Evaluation of the temperature T by using the MSI solver.
7. Calculation of density (both, inside the control volumes and at their faces), SIMPLEC coefficients and estimation of face velocities.
8. Discretization of the mass equation providing the coefficients and source-terms of an algebraic system. Evaluation of the pressure correction P' by using the MSI solver.
9. Correction of nodal pressures, face and nodal densities, and face and nodal velocities by using the pressure correction P' .
10. Return to item 8 until the achievement of the desired number of iterations.
11. In case of non-equilibrium flow model, the mass fractions Y_i should be obtained by the solution of an algebraic system by using the MSI method. For other multi-species models, the summation of mass fractions of all species must be equal to unity.
12. Return to item 2, until the achievement of the desired number of iterations or a tolerance.
13. Post-processing.

4. Numerical error analysis

Asymptotic (expected) convergence order, p_L , is evaluated by using an analysis based on the Taylor Series applied for the numerical interpolation schemes, which were employed in the discretization of the mathematical model. To estimate the apparent convergence order, p_U [34], three numerical solutions, φ_1 , φ_2 and φ_3 , are needed. These solutions are related to three different grids, named, respectively, as fine (Δx_1), coarse (Δx_2) and supercoarse (Δx_3), where Δx is the average volume size for the used grid. Thus, the obtained relation is:

$$p_U(\Delta x_1) = \frac{\log \left[\frac{(\varphi_2 - \varphi_3)}{(\varphi_1 - \varphi_2)} \right]}{\log(q)} \quad (8)$$

where q is the grid refinement ratio, taken as constant for all grids, defined as

$$q = \frac{\Delta x_2}{\Delta x_1} = \frac{\Delta x_3}{\Delta x_2} \quad (9)$$

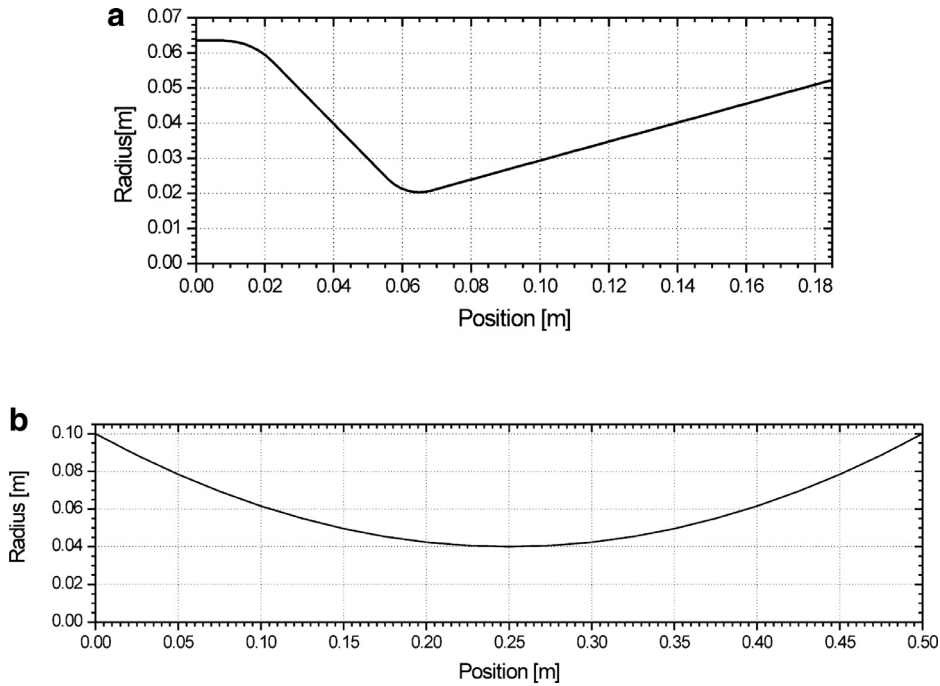


Fig. 1. Rocket engine nozzle profiles used for numerical simulations: (a) Geometry from Back et al. [37]; (b) Parabolic geometry.

Both asymptotic and apparent convergence orders are important for the evaluation of the GCI estimator [11] and the Richardson estimator [35–36], given by the following relations, respectively:

$$GCI(\varphi_1, p) = 3 \frac{|\varphi_1 - \varphi_2|}{(q^p - 1)} \quad (10)$$

and

$$U_{Ri}(\varphi_1, p) = \frac{(\varphi_1 - \varphi_2)}{(q^p - 1)} \quad (11)$$

where p assumes the lower value of p_L and p_U for the GCI estimator, and it can be either p_L or p_U , if the interest is in asymptotic or in apparent order, for the Richardson estimator.

5. Definition of the problem

The boundary conditions for flow of combustion gases, applied with ghost-cells, are:

- Entrance conditions: temperature (T) and pressure (P) are functions of the stagnation parameters; the chemical composition of the gas mixture, given by mass fractions (Y_i), is obtained from local data (temperature and pressure); this last item is not necessary for one-species models. The entrance axial velocity (u) is obtained from a linear extrapolation from the values obtained for internal flow. The radial velocity (v) is null.
- Nozzle walls: adiabatic.
- Exit conditions: for supersonic flows in nozzles, no exit boundary conditions are required; for the implementation of a numerical model, however, exit boundary conditions are needed. Because of this, temperature (T), axial and radial velocities (u and v), pressure (P) and mass fractions (Y_i) are obtained by linear extrapolation from internal control volumes.
- Symmetry line: symmetry conditions for all variables; null radial velocity.

For all simulations, two different geometries were chosen (shown in Fig. 1): the first one is presented by Back et al. [37], which presents a conical geometry and, for convenience, it will be cited as conical nozzle in this work; and the second one is a parabolic nozzle.

The global parameters of interest are: the nozzle discharge coefficient (C_d), the thrust for vacuum conditions (F) and the specific impulse (I_s), which are defined by

$$C_d = \frac{\dot{m}_{\text{exp}}}{\dot{m}_{\text{theor}}}; F = \int_{S_{\text{ex}}} \rho u^2 dS; I_s = \frac{\int_0^{t_b} F dt}{g \int_0^{t_b} \dot{m}_p dt} \quad (12)$$

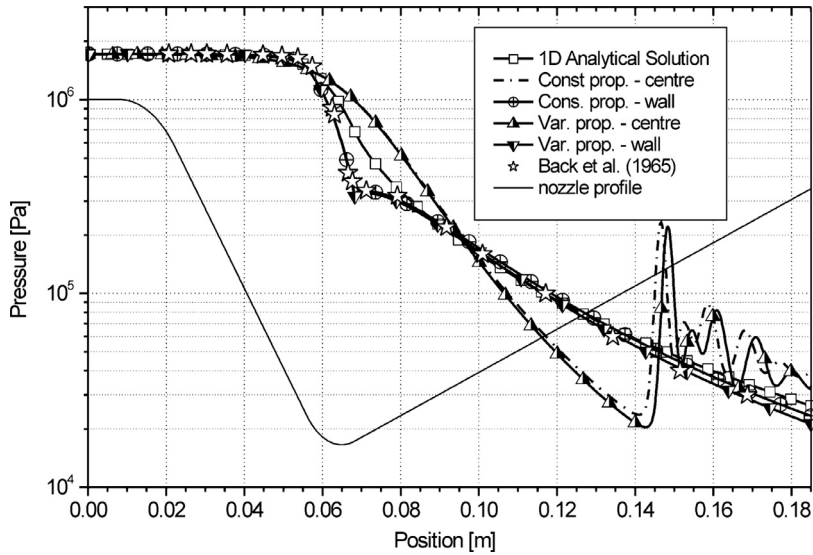


Fig. 2. Pressure distribution through the nozzle for air flow (720×80 control volumes, Problem 1).

where \dot{m}_{exp} is the numerical result for mass flow rate at nozzle, \dot{m}_{theor} is the isentropic one-dimensional mass flow rate for the same nozzle conditions, S_{ex} is the cross-section area at the nozzle exit, g is the gravitational acceleration, \dot{m}_p is the propellant mass flow rate and tb is the time interval of propellant burn-out.

6. Numerical results and discussion

6.1. Problem 1: Back et al. [37] geometry—code validation and verification

For the validation of the implemented code, experimental data provided by Back et al. [37] were employed. In this case, air was modeled as a one-species perfect gas, with the gas constant $R = 287.0 \text{ J/kg}\cdot\text{K}$ and ratio between specific heats, $\gamma = 1.35$. Furthermore, the other parameters/properties are: stagnation pressure of 1.725 MPa; stagnation temperature of 833.33 K; CDS interpolation scheme with deferred correction; 90×10 , 180×20 , 360×40 and 720×80 control volume grids (axial \times radial directions, respectively); and enough iterations to achieve the machine round-off error (which minimizes the iteration errors). The values of R and γ could be kept constant because, for this studied problem, the temperature gradient does not achieve extremely high values. In addition to constant air properties, variable properties were also studied and both results (constant and variable properties), for a 720×80 control volumes grid, are given in Fig. 2. When the one-species variable properties model is employed, the values of the specific heat at constant pressure (c_p) are dependent on the temperature, according to a polynomial fitting obtained by the use of tabulated data provided by Incropera et al. [38]. Comparing numerical to experimental pressure data, a good agreement between both results was observed, validating the implemented code. These results were previously reported by Araki and Marchi [39].

Another validation test, which was not done before in other works, for the implemented code was done for the same conical geometry. The experimental data, however, were the ones provided by Cuffel et al. [40]. In this case, values obtained for Mach number were compared for two regions: the wall and the centreline (symmetry line) of the rocket engine nozzle. In this case, air was modelled as a one-species perfect gas, with the ratio between specific heats, $\gamma = 1.40$. The stagnation pressure and temperature took values of, respectively, 482.6 kPa and 300 K. In this case, again, the values of R and γ could be kept constant because, for this studied problem, temperature gradient does not achieve extremely high values. Other numerical parameters were kept equal to the previous validation case. As can be seen in Fig. 3, there is a good concordance between numerical and experimental data at the nozzle symmetry line. The analytical Mach number over the symmetry line, at the nozzle throat, provided by Kliegel and Levine [41], was also included in Fig. 3: this analytical solution slightly overpredicts both numerical and experimental data.

In the vicinity of the wall, on the other hand, the concordance of numerical and experimental data is not so good. As exposed by Cuffel et al. [40], experimental data were obtained at a distance of about 1.8 mm from the nozzle wall. Because of this, two sets of numerical results are provided at Fig. 3: one correspondent to the Mach values exactly placed at the nozzle wall and the other one at a distance of 1.8 mm from the wall. Apparently, near-to-wall numerical results underpredict the experimental behaviour, especially in the region between -5 and $+5$ mm around the nozzle throat. It must be noted, however, that experimental data also presents uncertainties and the evaluation of the experimental Mach number is based actually on pressure measurements. As observed by Cuffel et al. [40], the true static pressure could be measured only when the flow was parallel to the used pitot-tube; at some locations, however, the flow was inclined to the tube. In this case, the

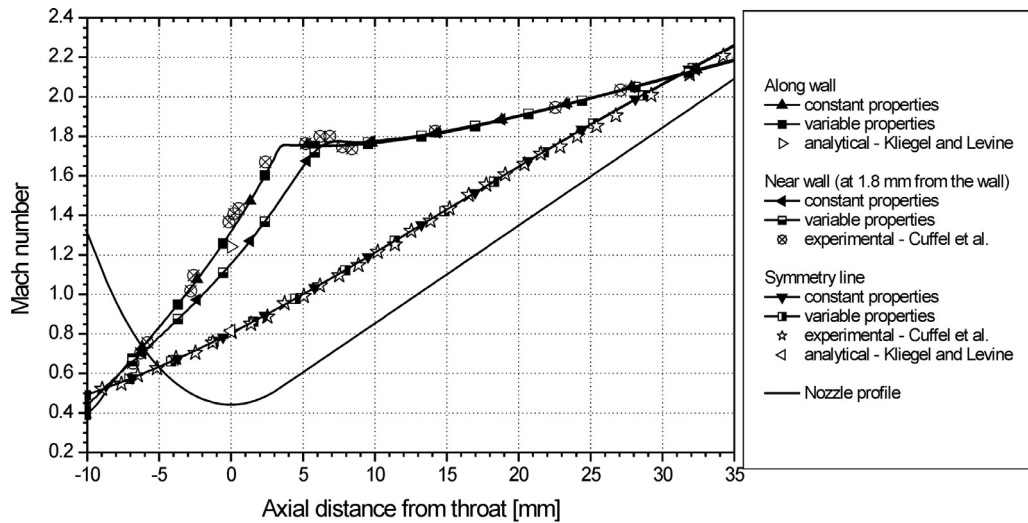


Fig. 3. Mach number distribution through the nozzle for air flow (720 × 80 control volumes, Problem 1) in the transonic region.

Table 3

Discharge coefficient for air flow through Back et al. [37] nozzle (720 × 80 grid, Problem 1).

Case 1:

Air flow, stagnation pressure of 1.725 MPa, stagnation temperature of 833.33 K, $\gamma = 1.35$.
 Analytical solution by Kliegel and Levine [41]: 0.982020.
 Experimental value by Back et al. [37]: 0.974 to 0.980

Physical model	UDS	CDS
One-species, constant properties	$0.99 \pm 2 \times 10^{-2}$ ($p_U \approx 0.93$)	$0.98169 \pm 2 \times 10^{-5}$ ($p_U \approx 2.74$)
One-species, variable properties	$0.99 \pm 2 \times 10^{-2}$ ($p_U \approx 0.93$)	$0.98428 \pm 2 \times 10^{-5}$ ($p_U \approx 2.93$)

Case 2:

Air flow, stagnation pressure of 482.6 kPa, stagnation temperature of 300 K, $\gamma = 1.40$.
 Analytical solution by Kliegel and Levine [41]: 0.981652
 Experimental value by Cuffel et al. [40]: 0.985 (average)

Physical model	UDS	CDS
One-species, constant properties	$0.99 \pm 2 \times 10^{-2}$ ($p_U \approx 0.92$)	$0.98140 \pm 2 \times 10^{-5}$ ($p_U \approx 2.29$)
One-species, variable properties	$0.99 \pm 2 \times 10^{-2}$ ($p_U \approx 0.92$)	$0.98108 \pm 2 \times 10^{-5}$ ($p_U \approx 2.28$)

pressure measured was lower than the true static pressure and a higher-than-true Mach number was calculated [40]. This could be the case of the Mach number at the near-to-wall region, especially around the nozzle throat, since it is the region in which the streamlines continually change their direction. Finally, comparing the numerical results and the experimental data to the analytical Mach number, it can be seen that the solution provided by Kliegel and Levine [41] underpredicts both the numerical and experimental results. Such behaviour is somewhat different than the one observed at the nozzle centreline (symmetry line).

A third validation test was made taking into account the Mach isolines, obtained for the throat region, using the previous test configuration. In this case, experimental data were the ones also provided by Cuffel et al [40] and are compared with numerical results for the UDS and CDS interpolation schemes in Fig. 4. As can be seen, both schemes present good concordance with experimental data, especially at the symmetry line. The sonic line is correctly captured by both interpolation schemes and both schemes also capture the oblique shock wave formation, although the UDS scheme tends to smooth this region by its diffusive behavior. Since numerical results in Fig. 4 are obtained by using an axisymmetric model, the sonic line does not exactly coincide with the nozzle throat [15,21]. The differences between the two interpolation schemes (UDS and CDS) are more evident for the near-to-wall region and for higher Mach numbers. In the subsonic region, both schemes present almost the same Mach profiles; though for the detection of the shock wave in the nozzle downstream region, more significant differences are noticeable and, in general, CDS results present a better agreement to the experimental data. These analyses were not made before.

Numerical error estimates, based on the GCI estimator, for the discharge coefficient were also analysed for both constant and variable air flows; the results are summarized in Table 3. As can be seen, numerical results for UDS interpolation scheme, with respective numerical error ranges, enclose those obtained using CDS scheme, as expected. It occurs because UDS presents first-order convergence rate while CDS shows second-order. However, it must be observed that the results for CDS one-species with constant properties do not enclose the analytical solution provided by Kliegel and Levine [41], which

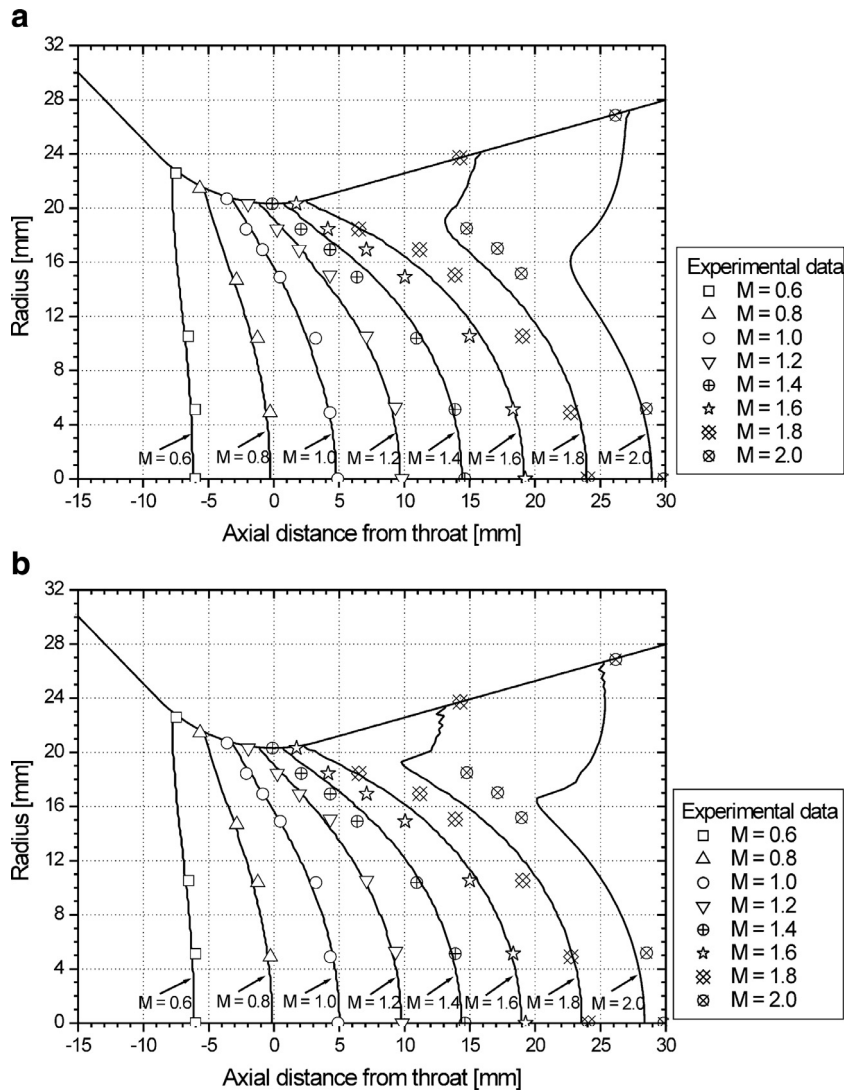


Fig. 4. Comparison of numerical and experimental Mach number distributions in the transonic region (720×80 control volumes, Problem 1). Numerical interpolation schemes: (a) UDS and (b) CDS.

was obtained for a flow of an irrotational perfect gas, using toroidal coordinates. The differences among both results could be related to the adopted model: for the numerical code, Euler equations for axisymmetric coordinates were employed. Euler equations correspond to a more realistic model than the irrotational flow for compressible gas flows [15].

Table 3 also provides experimental results obtained by Back et al. [37]. For Case 1, experimental results do not exactly match the analytical and/or the numerical ones. It must be noticed, however, that experimental results vary between 0.974 and 0.980 and do not include a range of experimental uncertainties. Because of this, and based on the fact that any device whose functionality is the measurement of flow parameters in supersonic flows can change the flow [15], it can be said that numerical results agree with experimental ones for Case 1.

Furthermore, despite the use of four different grids in both presented cases, only one apparent order could be evaluated, based on the triplet of grids 180×20 , 360×40 and 720×80 , for the CDS scheme. The obtained values were: for the first case, $p_U \approx 2.74$ for one-species, constant properties and $p_U \approx 2.93$ for one-species, variable properties, while for the second case, $p_U \approx 2.29$ for constant properties and $p_U \approx 2.28$ for variable properties; the asymptotic value, for all cases, was $p_L = 2$. On the other hand, the use of the same four grids allows the evaluation of two values for the apparent order, when the UDS scheme was employed; besides, the values of them are clearly close to the expected one, with $p_U \approx 0.93$ (or $p_U \approx 0.92$), for both physical models, in the finest grid.

The knowledge of only one value for the apparent order for the CDS scheme, although not too far from the asymptotic one, is not enough to assure that the apparent order converges monotonically to the expected/asymptotic one. In other words, it is not enough to guarantee that numerical solution belongs to the convergent interval [42], as required by the

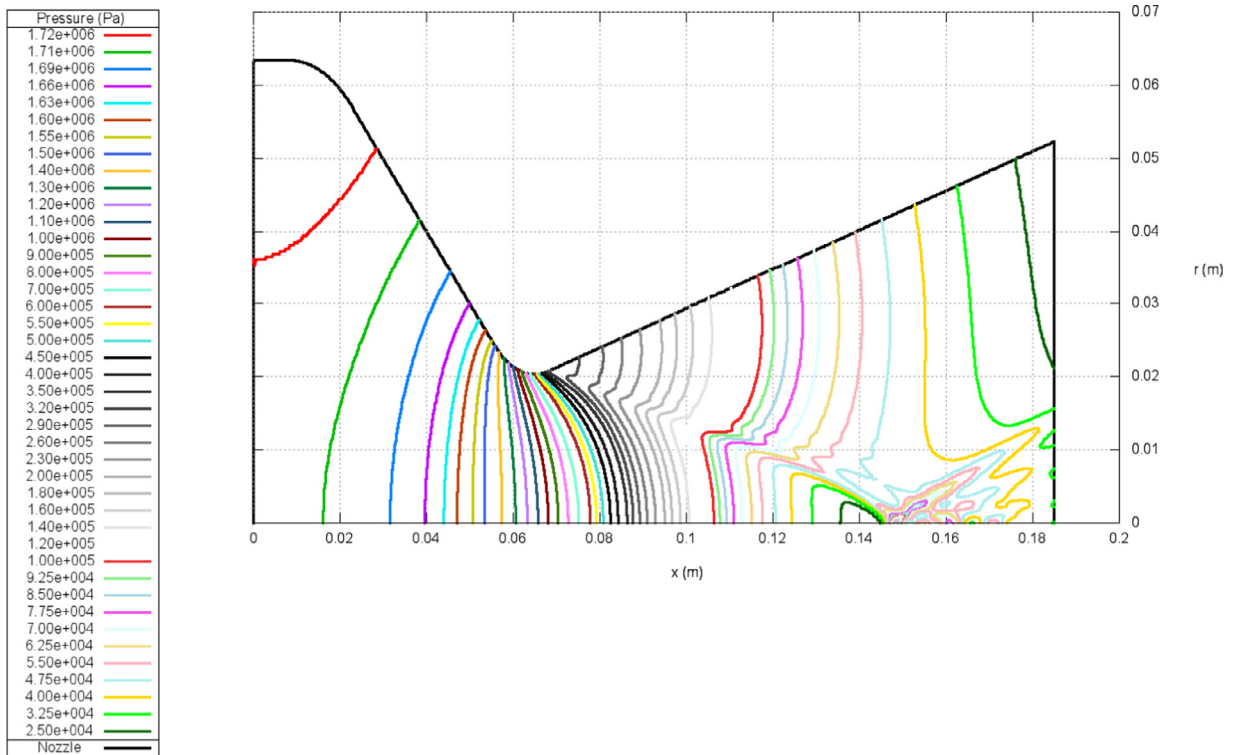


Fig. 5. Pressure isolines for Problem 1, showing the formation and detection of oblique shocks by Mach2D code.

Richardson and/or the GCI estimator. In cases in which the convergent interval is not observed, error estimators might result in inaccurate estimates as discussed by Roache [43]. The comparison among numerical and analytical results and the experimental data for the second case (which is an average value provided by Cuffel et al. [40]), however, shows that both numerical and analytical results present a good agreement to experimental data, which can provide another validation result.

The use of Euler equations is sufficient to guarantee the detection of oblique shocks by the numerical code. It can be seen, for example, in Fig. 5, in which isolines for pressure are shown. An oblique shock starts at the nozzle throat region and runs to the nozzle centreline, near the nozzle exit. Since the shock achieves the centreline, it is reflected originating another oblique shock, which runs to the nozzle exit. This behaviour is also observed for other thermophysical flow parameters, such as Mach number, temperature and/or density isolines, as can be seen at Fig. 6.

6.2. Problem 2. Parabolic nozzle—numerical verification

The second geometry employed was the parabolic one, presented in Fig. 1(b). At least 6 grids were used to provide numerical results for each chemical/physical model. It also allows the evaluation of both apparent order and error estimates (by GCI and Richardson estimators). Numerical results were obtained by using UDS and CDS with deferred correction, in order to allow the study of the influence of the chosen interpolation scheme on the error estimate. For all simulations the number of iterations was high enough to assure the achievement of the machine round-off error. For both frozen and local equilibrium flow models, tolerances associated to chemical reactions were posed as 10^{-12} for chemical dissociation rates, with the purpose of assuring convergence for the chemical reaction equations. These results were previously reported by Araki and Marchi [39].

Both frozen and local equilibrium flows are limit cases of the real reactive flow into a rocket engine nozzle [15,16]: while in the former model, the flow speed is much faster than the chemical reactions, for the latter model, reactions speed tend to infinity. Because of this, for frozen flow the chemical composition is kept unchanged from the nozzle inlet to its exit; and, for local equilibrium model, chemical equilibrium is achieved for each control volume of the flow. The behaviour of the apparent order, for global variables of interest, is shown in Fig. 7, while the error estimate, for specific impulse (I_S) is placed in Fig. 8. Both results refer to chemical model 4, for frozen flow and the following grids: 10×3 , 20×6 , 40×12 , 80×24 , 160×48 , 320×96 and 640×192 . Since in this case both temperature and pressure present strong variation along the nozzle, thermophysical properties are variable, except for one-species constant properties model.

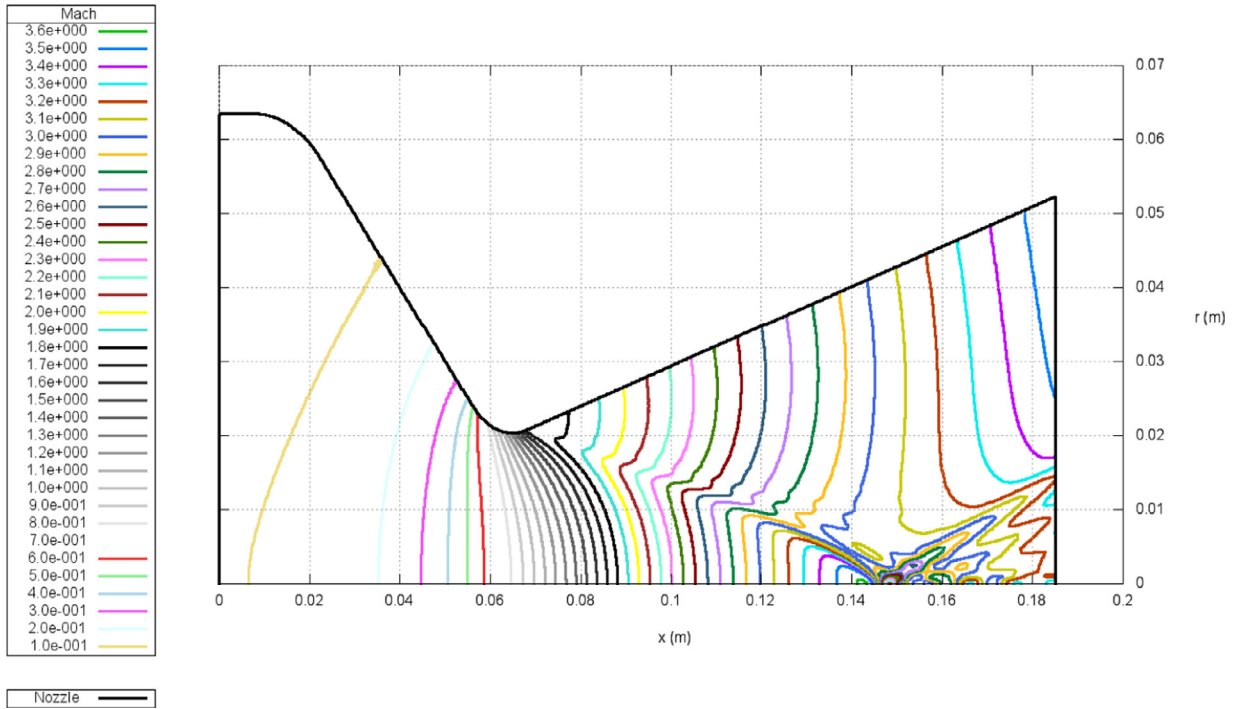


Fig. 6. Isolines for Mach number for Problem 1, showing the formation and detection of oblique shocks by Mach2D code.

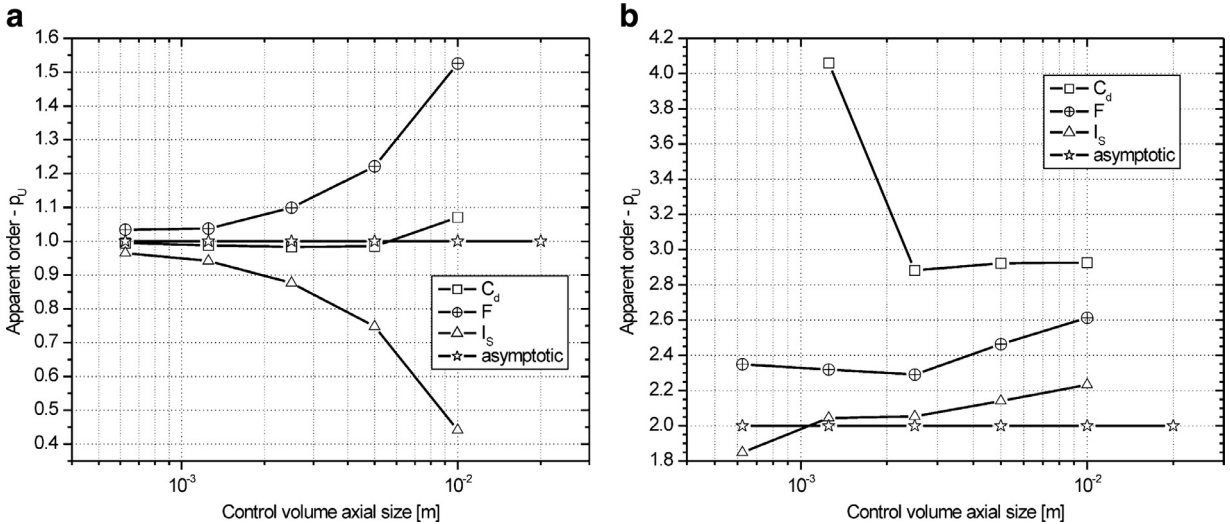


Fig. 7. Apparent order for (a) UDS and (b) CDS, frozen flow, model 4, Problem 2.

The physical parameters, which were considered to obtain numerical results presented in the current section are: stagnation pressure is equal to 1×10^6 Pa; stagnation temperature of 3420.33 K; ratio between specific heats and constant of gas (for one-species, constant properties model) of 1.1956 and 526.97 J/kg·K, respectively; oxidant/fuel ratio (for frozen, local equilibrium and non-equilibrium models) of about 7.9367 (stoichiometric ratio).

According to Fig. 7, the apparent order tends to the asymptotic one for UDS; for CDS, on the other hand, this tendency is yet unclear although the values are near 2. Such behaviour was observed not only for specific impulse but also for all other global variables of interest for the frozen flow model. However, local variables of interest (such as the exit temperature at symmetry line) have unclear tendency even for the UDS scheme. This behaviour might be associated both with chemical reaction and with variations of the values of properties. It could cause some instabilities in the tendency of convergence of numerical results and, consequently, in apparent order values.

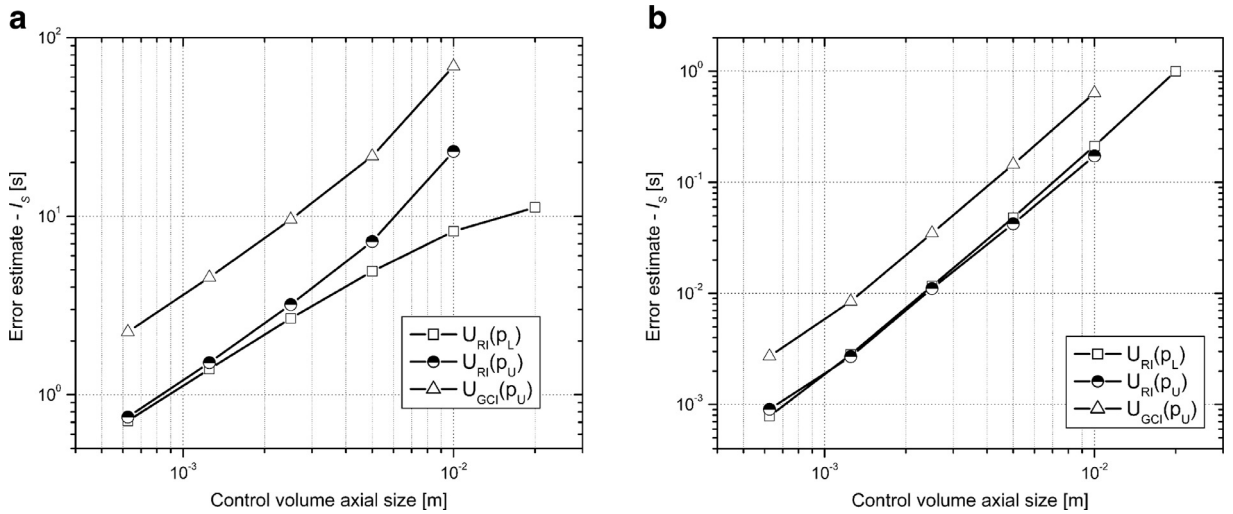


Fig. 8. Error estimate for (a) UDS and (b) CDS for I_s , frozen flow, model 4, Problem 2.

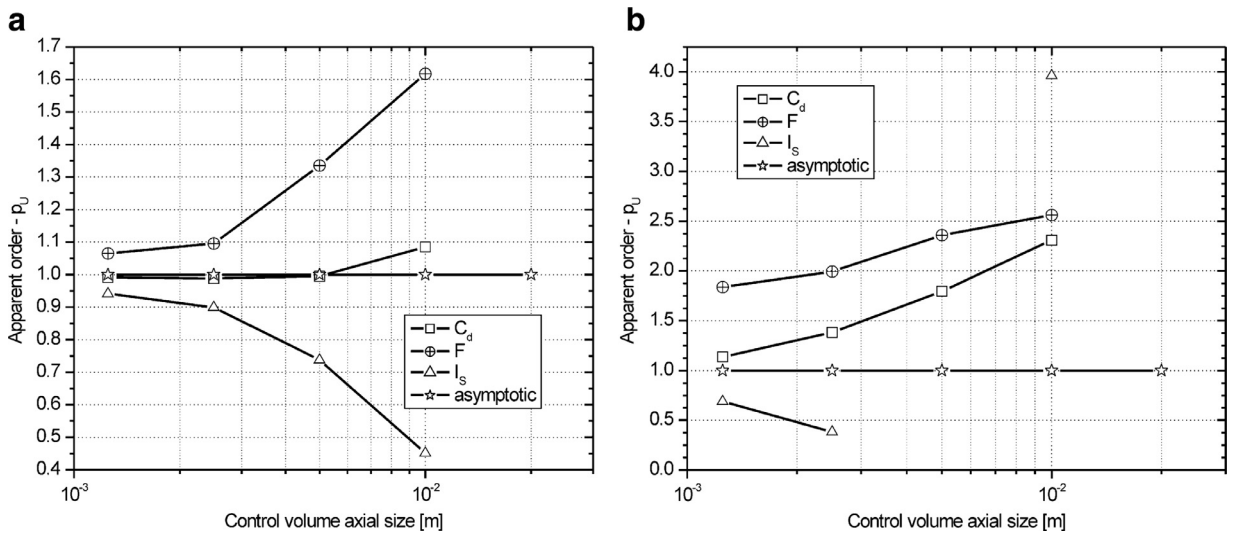


Fig. 9. Apparent order for (a) UDS and (b) CDS, equilibrium flow, model 4, Problem 2.

The error estimate for both Richardson and GCI estimators are shown at Fig. 8. Despite the unclear tendency for the apparent orders when CDS scheme is used, numerical error estimates are, at least three orders-of-magnitude smaller than the ones for UDS scheme, at the 640×192 grid. Based on this, it is recommended that the CDS scheme is used for frozen flow.

Local equilibrium flow results are presented in Figs. 9 and 10. Unlike the frozen flow model, apparent order has a tendency far from the forecasted value of 2. All variables of interest display apparent orders tending to unity. Each term of the governing equations was discretized using both UDS and CDS with deferred correction schemes, except for the chemical source term—Eq. 5(a). This term was discretized using the UDS scheme and, as can be seen by the numerical results, its inclusion degenerates the convergence order to unity. However, since almost all discretization components present approximations of second order, the related numerical error, when compared to the pure UDS scheme, is smaller. It influences the behaviour of numerical error estimates for CDS results, which are at least one order-of-magnitude smaller than the ones obtained with UDS, as can be seen at Fig. 10.

Tables 4 and 5 provide comparisons of physical and chemical models, as well as interpolation schemes (UDS and CDS with deferred correction). Such tables contain results previously obtained by Araki and Marchi [39]; such results, however, were confirmed since the numerical code was revised. Another observation is about the results provided for non-equilibrium flows, not available in [39]. All results include the GCI error estimates, except by H_2O -exit mass fraction for frozen flow models. The choice of GCI estimator is based on the recommendation of the ASME Standard for Verification and Validation [44]. The analytical solution of Kliegel and Levine [41] is also supplied for the discharge coefficient (C_d). Since this solution

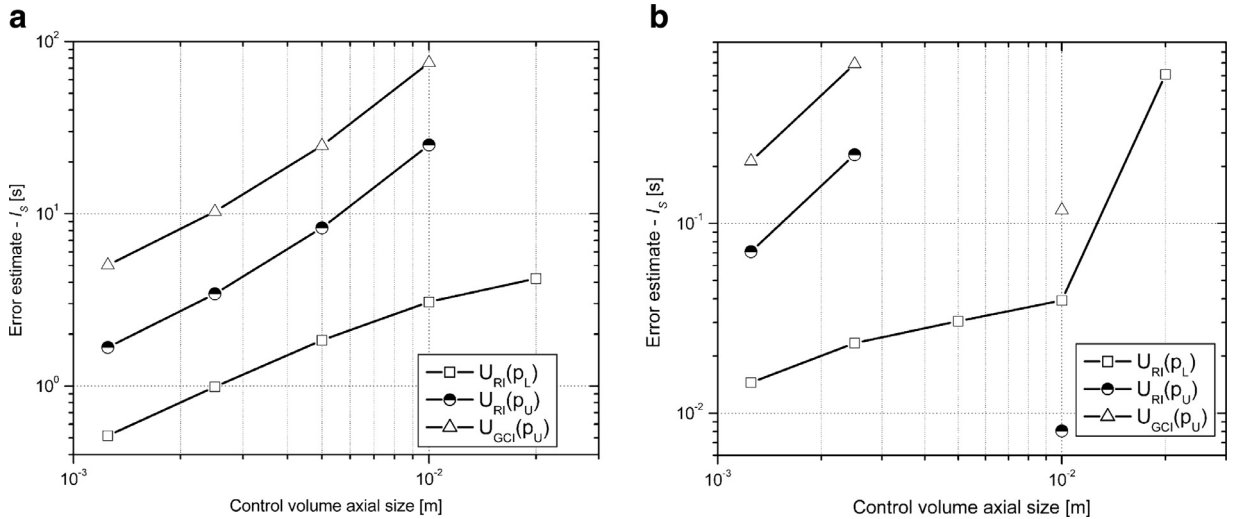


Fig. 10. Error estimate for (a) UDS and (b) CDS for I_s , equilibrium flow, model 4, Problem 2.

Table 4

Results for global variables of interest: C_d , F and I_s for the parabolic nozzle (320×96 grid, Problem 2).

Model	C_d (-)	F (N)	I_s (s)
UDS			
One-species, constant properties	$1.01 \pm 2 \times 10^{-2}$	$1.628 \times 10^4 \pm 8 \times 10^1$	$3.45 \times 10^2 \pm 5 \times 10^0$
One-species, variable properties	$1.00 \pm 2 \times 10^{-2}$	$1.635 \times 10^4 \pm 8 \times 10^1$	$3.45 \times 10^2 \pm 5 \times 10^0$
Frozen flow—mod. 4	$1.01 \pm 2 \times 10^{-2}$	$1.621 \times 10^4 \pm 9 \times 10^1$	$3.39 \times 10^2 \pm 5 \times 10^0$
Frozen flow—mod. 10	$1.01 \pm 2 \times 10^{-2}$	$1.621 \times 10^4 \pm 8 \times 10^1$	$3.39 \times 10^2 \pm 5 \times 10^0$
Equilibrium flow—mod. 4	$0.98 \pm 1 \times 10^{-2}$	$1.665 \times 10^4 \pm 7 \times 10^1$	$3.56 \times 10^2 \pm 5 \times 10^0$
Equilibrium flow—mod. 10	$0.98 \pm 2 \times 10^{-2}$	$1.665 \times 10^4 \pm 7 \times 10^1$	$3.56 \times 10^2 \pm 5 \times 10^0$
Non-equilibrium flow—mod. 3, variant 1 [25]	$1.06 \pm 2 \times 10^{-2}$	$1.651 \times 10^4 \pm 8 \times 10^1$	$3.27 \times 10^2 \pm 4 \times 10^0$
Non-equilibrium flow—mod. 3, variant 2 [26]	$1.07 \pm 2 \times 10^{-2}$	$1.654 \times 10^4 \pm 8 \times 10^1$	$3.25 \times 10^2 \pm 4 \times 10^0$
CDS with deferred correction			
One-species, constant properties	$0.999876 \pm 2 \times 10^{-6}$	$1.62516 \times 10^4 \pm 4 \times 10^{-1}$	$3.41743 \times 10^2 \pm 8 \times 10^{-3}$
One-species, variable properties	$0.991678 \pm 4 \times 10^{-6}$	$1.632442 \times 10^4 \pm 8 \times 10^{-2}$	$3.46111 \times 10^2 \pm 3 \times 10^{-3}$
Frozen flow—mod. 4	$1.000962 \pm 2 \times 10^{-6}$	$1.61859 \times 10^4 \pm 4 \times 10^{-1}$	$3.39993 \times 10^2 \pm 8 \times 10^{-3}$
Frozen flow—mod. 10	$1.000970 \pm 2 \times 10^{-6}$	$1.61860 \times 10^4 \pm 4 \times 10^{-1}$	$3.39991 \times 10^2 \pm 8 \times 10^{-3}$
Equilibrium flow—mod. 4	$0.9785 \pm 5 \times 10^{-4}$	$1.6625 \times 10^4 \pm 3 \times 10^0$	$3.572 \times 10^2 \pm 2 \times 10^{-1}$
Equilibrium flow—mod. 10	$0.9785 \pm 5 \times 10^{-4}$	$1.6625 \times 10^4 \pm 3 \times 10^0$	$3.572 \times 10^2 \pm 2 \times 10^{-1}$
Kliegel and Levine [41]—2D analytical solution for irrotational, one-species, constant properties flow	0.999877	—	—

Table 5

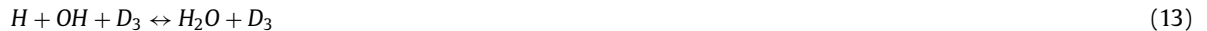
Results for local variables of interest: P_{ex} , T_{ex} , u_{ex} and $Y(H_2O)_{ex}$ (at symmetry line), for the parabolic nozzle (320×96 grid, Problem 2).

Model	P_{ex} (Pa)	T_{ex} (K)	u_{ex} (m/s)	$Y(H_2O)_{ex}$ (-)
UDS				
One-species, constant properties	$7.2 \times 10^4 \pm 7 \times 10^3$	$1.99 \times 10^3 \pm 4 \times 10^1$	$3.03 \times 10^3 \pm 5 \times 10^1$	—
One-species, variable properties	$7 \times 10^4 \pm 1 \times 10^4$	$2.09 \times 10^3 \pm 4 \times 10^1$	$3.06 \times 10^3 \pm 6 \times 10^1$	—
Frozen flow—mod. 4	$6.9 \times 10^4 \pm 3 \times 10^3$	$1.92 \times 10^3 \pm 3 \times 10^1$	$3.03 \times 10^3 \pm 5 \times 10^1$	0.783686
Frozen flow—mod. 10	$6.9 \times 10^4 \pm 2 \times 10^3$	$1.92 \times 10^3 \pm 3 \times 10^1$	$3.03 \times 10^3 \pm 4 \times 10^1$	0.783539
Equilibrium flow—mod. 4	$8.3 \times 10^4 \pm 3 \times 10^3$	$2.64 \times 10^3 \pm 1 \times 10^1$	$3.10 \times 10^3 \pm 5 \times 10^1$	$0.902 \pm 2 \times 10^{-3}$
Equilibrium flow—mod. 10	$8.3 \times 10^4 \pm 2 \times 10^3$	$2.64 \times 10^3 \pm 1 \times 10^1$	$3.10 \times 10^3 \pm 5 \times 10^1$	$0.902 \pm 2 \times 10^{-3}$
Non-equilibrium flow—mod. 3, variant 1 [25]	$7.6 \times 10^4 \pm 2 \times 10^3$	$2.06 \times 10^3 \pm 3 \times 10^1$	$2.89 \times 10^3 \pm 4 \times 10^1$	$0.8614 \pm 4 \times 10^{-4}$
Non-equilibrium flow—mod. 3, variant 2 [26]	$7.7 \times 10^4 \pm 2 \times 10^3$	$2.07 \times 10^3 \pm 2 \times 10^1$	$2.87 \times 10^3 \pm 4 \times 10^1$	$0.8794 \pm 6 \times 10^{-4}$
CDS with deferred correction				
One-species, constant properties	$7.14 \times 10^4 \pm 9 \times 10^2$	$1.98 \times 10^3 \pm 1 \times 10^1$	$3.04 \times 10^3 \pm 2 \times 10^1$	—
One-species, variable properties	$7.34 \times 10^4 \pm 9 \times 10^2$	$2.083 \times 10^3 \pm 7 \times 10^0$	$3.07 \times 10^3 \pm 1 \times 10^1$	—
Frozen flow—mod. 4	$6.90 \times 10^4 \pm 9 \times 10^2$	$1.91 \times 10^3 \pm 2 \times 10^1$	$3.04 \times 10^3 \pm 5 \times 10^1$	0.783686
Frozen flow—mod. 10	$6.90 \times 10^4 \pm 9 \times 10^2$	$1.91 \times 10^3 \pm 2 \times 10^1$	$3.04 \times 10^3 \pm 5 \times 10^1$	0.783539
Equilibrium flow—mod. 4	$8.31 \times 10^4 \pm 8 \times 10^2$	$2.6345 \times 10^3 \pm 3 \times 10^{-1}$	$3.113 \times 10^3 \pm 5 \times 10^0$	$0.903 \pm 1 \times 10^{-3}$
Equilibrium flow—mod. 10	$8.31 \times 10^4 \pm 8 \times 10^2$	$2.6347 \times 10^3 \pm 3 \times 10^{-1}$	$3.113 \times 10^3 \pm 5 \times 10^0$	$0.903 \pm 1 \times 10^{-3}$

was obtained by considering the hypothesis of a perfect gas flow with constant properties, it allows the comparison to the “one-species, constant properties” model.

By comparing results in Tables 4 and 5, numerical results obtained by using CDS are always smaller than the ones by using the UDS counterparts. In all cases and for all variables of interest, the range of error estimates with UDS scheme encloses the CDS ones, except for the thrust evaluated with the local equilibrium model. In this case, there is an intersection zone between both results (UDS and CDS); however they do not coincide in the whole interval. It is probably caused by the degeneration of apparent orders for all variables of interest observed for the CDS, as can be seen at Fig. 9.

Although Tables 4 and 5 present only numerical results for models 4 (6 species model) and 10 (8 species model) for both frozen and equilibrium flows, it must be observed that numerical results for models 3, 5 and 7 are coincident to the ones of model 4, as well as results for model 9 is equal to the ones of model 10. Tables 4 and 5 also provide results for non-equilibrium flows, for chemical model 3; it must be noted, however, that this model presents 2 variants: although both share the same chemical species and same dissociation reactions, the rates of direct reaction and the efficiency of third bodies are different for both variants. For example, one of the dissociation reactions associated to model 3 is



In this case, D_3 represents the third body, which can be any of the species considered in the chemical model. According Barros et al. [25], for this reaction, for example, all six species (H_2 , O_2 , H_2O , OH , H and O) present the same efficiency to catalyze this partial reaction; however, after Smith et al. [26], each species presents a different efficiency to the same reaction. Since the efficiency of third bodies in partial dissociation reactions are very difficult to evaluate, this work presents numerical results for model 3 using the efficiencies provided by both authors, Barros et al. [25]—which is named in this work “variant 1”—and Smith et al. [26], which is named “variant 2”.

Based on the numerical results presented in Tables 4 and 5 some comparisons can be done for the different physical models. To start with, it can be observed that the differences among physical models are relatively small for all global variables of interest: it corresponds only to 9.1% for discharge coefficient, 2.7% for thrust and 9.5% for specific impulse. For local variables of interest, on the other hand, these discrepancies are more appreciable: 20.4% for exit pressure and 37.9% for exit temperature (at symmetry line). However the axial exit velocity is less influenced by physical model, since the observed variation between the extreme values is about 8.0%.

One interesting conclusion that can be drawn by comparing chemical models involving six and eight species is that both cases present similar results. It is an important remark because a six species model needs much smaller computational processing requirements. For example, for the 320×96 grid with CDS scheme and for local equilibrium flow: the six species model required 13.6 hours for convergence, while the eight species model demanded 21.3 hours (57.3% more) to achieve the same criteria (30,000 iterations, which was enough to achieve the round-off error).

By comparing the processing time (CPU time) requirements for chemical six species models, it was observed that: the frozen flow model needed about 2.5 hours, the local equilibrium flow about 14 hours and the non-equilibrium flow about 6 to 6.6 days. Based on these pieces of information, it is recommended to use the frozen and local equilibrium flow analysis, at least for a first evaluation in rocket engine projects.

Numerical results presented in Tables 4 and 5 can be useful to validate numerical codes, providing a benchmark for reactive and non-reactive non-viscous flows.

7. Conclusion

Verification and validation of a numerical code for two-dimensional, non-viscous, one- or multi-species flows were presented in this paper. Numerical results for air flow through a conical geometry rocket engine nozzle were compared to the experimental data provided by Back et al. [37] for pressure, and by Cuffel et al. [40] for Mach numbers, showing good agreement and validating the code. The two-dimensional code was also able to detect an oblique shock, which is formed in the region of the nozzle throat and travels along the flow, being reflected near the exit region of the nozzle, as expected.

A second geometry (a parabolic one) was employed to provide benchmark results for reactive and non-reactive flows. In this case, apparent orders, Richardson and GCI error estimators were evaluated to all numerical results. First order (UDS) and second order (CDS with deferred correction) interpolation schemes were employed in the discretization of the governing equations. For both geometries, numerical results for apparent orders of convergence agreed well with the asymptotic (expected) ones for one-species flows. Some other analyses were provided for mixture of gases flows; in this case, for frozen flow, the apparent order values tend to the asymptotic ones in all cases; for local equilibrium flow, the use of CDS degenerated the apparent order to unity; this fact can be associated to the use of UDS interpolation scheme in the source term of the energy equation. Since numerical results of grid convergence tests for the conical geometry nozzle presents a similar behaviour, they were not included in this work.

Global variables of interest, which are related to the rocket performance, present smaller influence of the choice of physical model (variations are about 10%), while local variables of interest are more affected by this kind of choice (variations can achieve about 40% for temperature). The use of six or eight species models, however, has nearly null effect on numerical results. In fact, results are numerically equivalent and, based on the CPU time requirements, the use of six species models are encouraged.

Acknowledgements

The authors would acknowledge the Federal University of Paraná (UFPR), the Department of Mechanical Engineering (DEMEC) and the “UNIESPAÇO Program” of The Brazilian Space Agency (AEB) by physical and financial support given for this work. The first author would, also, grant the support provided by the Laboratory of Numerical Experimentation (LENA), and was supported by a scholarship of CAPES (Coordenação de Aperfeiçoamento de Pessoal de Nível Superior)—Brazil. The second author is supported by a scholarship of CNPq (Conselho Nacional de Desenvolvimento Científico e Tecnológico)—Brazil. The authors would also acknowledge the journal editor and reviewers by their suggestions and corrections.

References

- [1] D.K. Huzel, D.H. Huang, *Modern Engineering for Design of Liquid-Propellant Rocket Engines*, AIAA Progress in Astronautics and Aeronautics, Washington, 1992.
- [2] D. Kuhl, J. Riccius, O.J. Haidn, Thermomechanical analysis and optimization of cryogenic liquid rocket engines, *J. Propul. Power* 18 (2002) 835–846.
- [3] M.H. Naraghi, S. Dunn, D. Coats, A model of design and analysis of regeneratively cooled rocket engines, in: *Proceedings of the Joint Propulsion Conference, AIAA, Fort Lauderdale, USA, 2004*, pp. 2004–3852.
- [4] T.S. Wang, Multidimensional unstructured-grid liquid rocket-engine nozzle performance and heat transfer analysis, *J. Propul. Power* 22 (1) (2006) 78–84.
- [5] H.W. Zhang, W.Q. Tao, Y.L. He, W. Zhang, Numerical study of liquid film cooling in a rocket combustion chamber, *Int. J. Heat Mass Transfer* 49 (2006) 349–358.
- [6] T.S. Wang, Transient three-dimensional startup side load analysis of a regeneratively cooled nozzle, *Shock Waves* 19 (2009) 251–264.
- [7] X.D. Zhang, D. Pelletier, J.Y. Trépanier, R. Camarero, Numerical assessment of error estimators for Euler equations, *AIAA J.* 39 (2001) 1706–1715.
- [8] W.L. Oberkampf, T.G. Trucano, Verification and validation benchmarks, *Nucl. Eng. Des.* 238 (2008) 716–743.
- [9] U.B. Metha, Guide to credible computer simulations of fluid flows, *J. Propul. Power* 12 (5) (1996) 940–948.
- [10] P.J. Roache, *Verification and Validation in Computational Science and Engineering*, Hermosa Publishers, Albuquerque, 1998.
- [11] P.J. Roache, Perspective: a method for uniform reporting of grid refinement studies, *J. Fluids Eng.* 116 (1994) 405–413.
- [12] H.K. Versteeg, W. Malalasekera, *An Introduction to Computational Fluid Dynamics—The Finite Volume Method*, second ed., Prentice Hall, Harlow, 2007.
- [13] C.H. Marchi, C.R. Maliska, A nonorthogonal finite volume method for the solution of all speed flows using co-located variables, *Numer. Heat Transfer – Part B* 26 (1994) 293–311.
- [14] J.H. Ferziger, M. Perić, *Computational Methods for Fluid Dynamics*, third ed., Springer-Verlag, Berlin, 2001.
- [15] J.A. Anderson, *Modern Compressible Flow*, third ed., McGraw-Hill, Boston, 2003.
- [16] J.A. Anderson, *Hypersonic and High-Temperature Gas Dynamics*, second ed., AIAA Education Series, Reston, 2006.
- [17] G.P. Sutton, O. Biblarz, *Rocket Propulsion Elements*, eighth ed., John Wiley & Sons, Hoboken, 2010.
- [18] A. Fröhlich, M. Popp, G. Schmidt, D. Thelemann, Heat transfer characteristics of H₂/O₂ combustion chambers, in: *Proceedings of the Twenty-Ninth Joint Propulsion Conference, AIAA, Monterrey, USA, 1993*, pp. 93–1826.
- [19] M. Habiballah, L. Vingert, P. Vuillermoz, Research as a key in the design methodology of liquid-propellant combustion devices, *J. Propul. Power* 14 (5) (1998) 782–788.
- [20] C.H. Marchi, F. Laroca, A.F.C. Silva, J.N. Hinckel, Numerical solutions of flows in rocket engines with regenerative cooling, *Numer. Heat Transfer—Part A* 45 (2004) 699–717.
- [21] J.E. John, T.G. Keith, *Gas Dynamics*, third ed., Pearson Prentice Hall, New Jersey, 2006.
- [22] Bird R.B., Stewart W.E., Lightfoot E.N. *Transport Phenomena*, second ed. John Wiley & Sons, New York, 2002.
- [23] J.Y. Murthy, S.R. Mathur, A conservative numerical scheme for the energy equation, *J. Heat Transfer* 20 (4) (1998) 1081–1086.
- [24] B.J. McBride, S. Gordon, M.A. Reno, *Coefficients for Calculating Thermodynamic and Transport Properties of Individual Species, Coefficients for Calculating Thermodynamic and Transport Properties of Individual Species*, vol. 4513, NASA Lewis Center, Cleveland, 1993 NASA Technical Memorandum.
- [25] J.E.M. Barros, G.F. Alvim Filho, P. Paglione, 1990, Study of reactive flow in non-equilibrium through convergent-divergent nozzles (in Portuguese), in: *Proceedings of the Third National Meeting of Thermal Sciences (ENCIT)*, Itapema, Brazil, 1994.
- [26] T.A. Smith, A.J. Pavli, K.J. Kacynski, Comparison of Theoretical and Experimental Thrust Performance of a 1030: 1 Area Ratio Rocket Nozzle at a Chamber Pressure of 2413 kN/m² (350 psia), NASA Lewis Research Center, Cleveland, 1987 *NASA Technical Paper* 2725.
- [27] R.A. Svehla, Thermodynamic and Transport Properties for the Hydrogen-Oxygen System, NASA Lewis Center, Cleveland, 1964 *NASA SP-3011*.
- [28] R.J. Kee, J.F. GrCar, M.D. Smooke, J.A. Miller, A Fortran Program For Modeling Steady Laminar One-Dimensional Premixed Flames, Sandia National Laboratories, Albuquerque, 1990 *SAND85-8240•UC-401*.
- [29] C.H. Marchi, L.K. Araki, F. Laroca, Evaluation of thermochemical properties and combustion temperatures for LOX/LH₂ reaction schemes, in: *Proceedings of the Twenty-Sixth Iberian Latin-American Congress on Computational Methods in Engineering*, Guarapari, Brazil, 2005.
- [30] L.K. Araki, C.H. Marchi, Numerical solution of an one-dimensional reactive flow in a regeneratively rocket engine nozzle, in: *Proceedings of the Eleventh Brazilian Congress of Thermal Sciences and Engineering*, Curitiba, Brazil, 2006.
- [31] G.E. Schneider, M. Zedan, A modified strongly implicit procedure for the numerical solution of field problems, *Numer. Heat Transfer* 4 (1981) 1–19.
- [32] J.P. Van Doormaal, G.D. Raithby, Enhancements of the SIMPLE method for predicting incompressible fluid flow, *Numer. Heat Transfer* 7 (1984) 147–163.
- [33] I. Demirdzic, Z. Lilek, M. Peric, A collocated finite volume method for predicting flows at all speeds, *Int. J. Numer. Methods Fluids* 16 (1993) 1029–1050.
- [34] C.H. Marchi, A.F.C. Silva, Multi-dimensional discretization error estimation for convergent apparent order, *J. Braz. Soc. Mech. Sci. Eng.* 27 (4) (2005) 432–439.
- [35] L.F. Richardson, The approximate numerical solution by finite differences of physical problems involving differential equations, with an application to the stresses in a masonry dam, *Philos. Trans. R. Soc. London—Ser. A* 210 (1910) 307–357.
- [36] L.F. Richardson, J.A. Gaunt, The deferred approach to the limit, *Philos. Trans. R. Soc. London—Ser. A* 227 (1927) 299–361.
- [37] L.H. Back, P.F. Massier, H.L. Gier, Comparison of measured and predicted flows through conical supersonic nozzles, with emphasis on the transonic region, *AIAA J.* 3 (9) (1965) 1606–1614.
- [38] F.P. Incropera, D.P. DeWitt, T.L. Bergman, A.S. Lavine, *Fundamentals of Heat and Mass Transfer*, sixth ed., John Wiley & Sons, New York, 2007.
- [39] L.K. Araki, C.H. Marchi, Verification of numerical solution of two-dimensional reactive flow in rocket engine nozzles, in: *Proceedings of the Nineteenth International Congress of Mechanical Engineering*, Brasilia, Brazil, 2007.
- [40] R.F. Cuffel, L.H. Back, P.F. Massier, Transonic flow in a supersonic nozzle with small throat radius of curvature, *AIAA J.* 7 (1969) 1364–1366.
- [41] J.R. Kliegel, J.N. Levine, Transonic flow in small throat radius of curvature nozzle, *AIAA J.* 7 (1969) 1375–1378.
- [42] C.H. Marchi, A.F.C. Silva, Unidimensional numerical solution error estimation for convergent apparent order, *Numer. Heat Transfer—Part B* 42 (2) (2002) 167–188.
- [43] P.J. Roache, Discussion: “factors of safety for richardson extrapolation”, *J. Fluids Eng.* 133 (2011) 115501.
- [44] ASME, *Standard for Verification and Validation in Computational Fluid Dynamics and Heat Transfer*. ASME V&V 20-2009. 2009.